

Constrained Optimization to Train Neural Networks on Critical and Under-Represented Classes

Sara Sangalli¹, Ertunc Erdil¹, Andreas Hoetker², Olivio Donati², Ender Konukoglu¹

¹ Computer Vision Lab, ETH Zürich

² Institute for Diagnostic and Interventional Radiology, Universitätsspital Zürich
sara.sangalli@vision.ee.ethz.ch

Abstract

Deep neural networks (DNNs) are notorious for making more mistakes for the classes that have substantially fewer samples than the others during training. Such class imbalance is ubiquitous in clinical applications and very crucial to handle because the classes with fewer samples most often correspond to critical cases (e.g., cancer) where misclassifications can have severe consequences. Not to miss such cases, binary classifiers need to be operated at high True Positive Rates (TPRs) by setting a higher threshold, but this comes at the cost of very high False Positive Rates (FPRs) for problems with class imbalance. Existing methods for learning under class imbalance most often do not take this into account. We argue that prediction accuracy should be improved by emphasizing reducing FPRs at high TPRs for problems where misclassification of the positive, i.e. critical, class samples are associated with higher cost. To this end, we pose the training of a DNN for binary classification as a constrained optimization problem and introduce a novel constraint that can be used with existing loss functions to enforce maximal area under the ROC curve (AUC) through prioritizing FPR reduction at high TPR. We solve the resulting constrained optimization problem using an Augmented Lagrangian method (ALM). Going beyond binary, we also propose two possible extensions of the proposed constraint for multi-class classification problems. We present experimental results for image-based binary and multi-class classification applications using an in-house medical imaging dataset, CIFAR10, and CIFAR100. Our results demonstrate that the proposed method improves the baselines in majority of the cases by attaining higher accuracy on critical classes while reducing the misclassification rate for the non-critical class samples.¹

1 Introduction

Deep Neural Networks (DNNs) perform extremely well in many classification tasks when sufficiently large and representative datasets are available for training. However, in many real world applications, it is not uncommon to encounter highly-skewed class distributions, i.e., majority of the data belong to only a few classes while some classes are represented with scarce instances. Training DNNs on such imbalanced datasets leads to models that are biased toward majority classes with poor prediction accuracy for the minority class’ samples. While this is problematic for all such applications, it poses an even greater issue for “critical” applications where misclassifying samples belonging to the minority class can have severe consequences. One domain where such applications are common and machine learning is having an important impact is medical imaging.

In medical imaging, applications with data imbalance are ubiquitous [24] and costs of making some types of mistakes are more severe than others. For instance, in a diagnosis application, discarding a

¹Code is available at: <https://github.com/salusanga/alm-dnn>.

cancer case as healthy (False Negative) is more costly than classifying a healthy subject as having cancer (False Positive). While the latter creates burden for the subject as well as health-care system through additional tests that may be invasive and expensive, the former, i.e., failure to identify a cancerous case, would delay the diagnosis and jeopardise treatment success. In such applications, binary classifiers are operated at high True Positive Rates (TPRs) even when this means having higher False Positive Rates (FPRs). To make matters more complicated, there are usually significantly fewer samples to represent critical classes, where mistakes are more severe. For instance, in [10] authors found out that in prostate cancer screening only 30% of even the most suspicious cases identified with initial testing actually have cancer. Such class imbalance increases the FPR even higher in “critical” applications, because the models tend to misclassify minority classes more often. Useful algorithms need to achieve low FPR at high TPR operating points, even under class imbalance.

While various methods for learning with imbalanced datasets exist, to the best of our knowledge, these methods do not take into account the fact that “critical” applications need to be operated at high accuracy for the critical classes. We believe that for such applications ensuring low misclassification rate for the non-critical samples and high accuracy for the critical classes should be the main goal, to make binary classifiers useful in practice. This motivates us to design new strategies for training DNNs for classification.

Contribution: In this paper, we pose the training of a DNN for binary classification under class imbalance as a constrained optimization problem and propose a novel constraint that can be used with existing loss functions. We define the constraint using Mann-Whitney statistics [27] in order to maximize the AUC, but in an asymmetric way to favor reduction of false positives at high true positive (or low false negative) rates. Then, we transfer the constrained problem to its dual unconstrained optimization problem using an Augmented Lagrangian method (ALM) [2]. We optimize the resulting loss function using stochastic gradient descent. Unlike the existing methods that directly optimize AUC, we incorporate AUC optimization in a principled way into a constrained optimization framework. We finally present two possible extensions of the proposed constraint for multi-class classification problems.

We present an extensive evaluation of the proposed method for image-based binary and multi-class classification problems on three datasets: an in-house medical dataset for prostate cancer, CIFAR10, and CIFAR100 [19]. In all datasets, we perform experiments by simulating different class imbalance ratios. In our experiments, we apply the proposed constraint to 9 different baseline loss functions, most of which were proposed to handle class imbalance. We compare the results with the baselines without any constraint. The results demonstrate that the proposed method improves the baselines in majority of the cases.

2 Related work

Various methods have already been proposed to learn better models with class-imbalanced datasets. We group the existing methods into three categories: cost sensitive training-based methods, sampling-based and classifier-based methods. Here, we focus on the first one and present related work for the other groups in the supplementary material for space reasons.

Cost sensitive training-based methods: This family of methods aims at handling class imbalance by designing an appropriate loss function to be used during training. In particular, they design the loss functions to give more emphasis to the minority class’ samples, or the class with higher associated risk, than the majority ones during training [34]. [38] proposes a loss function, which we refer to as Weighted BCE (W-BCE), where minority class’ samples are multiplied by a constant to introduce more cost to misclassification of those samples. [18] proposes a function that aims to learn more discriminative latent representations by enforcing DNNs to maintain inter-cluster and inter-class margins, where clusters are formed using k-means clustering. They demonstrate that the tighter constraint inherently reduces class imbalance. In a more recent work, [8] proposes a loss function called class-balanced binary cross-entropy (CB-BCE) to weight BCE inversely proportionally to the class frequencies to amplify the loss for the minority class’ samples. In a similar vein, [23] modifies BCE and propose symmetric focal loss (S-FL) by multiplying it with the inverse of the prediction probability to introduce more cost to the samples that DNNs are not very confident. [25] introduces symmetric margin loss (S-ML) by introducing a margin to the BCE loss. [22] investigates different loss functions such as S-FL and S-ML, and propose their asymmetric versions, A-FL and

A-ML, by introducing a margin for the minority class' samples to handle class imbalance. In a different line of work, [36] proposes a method called mean squared false error by performing simple yet effective modification to the mean squared error (MSE) loss. Unlike MSE, which computes an average error from all samples without considering their classes, this loss computes a mean error for each class and averages them. [4] proposes a label-distribution-aware margin (LDAM) loss motivated by minimizing a margin-based generalization bound, optionally coupled with a training schedule that defers re-weighting until after the initial stage. [30] introduces balanced meta-softmax for long-tailed recognition, which accommodates the label distribution shift between training and testing, as well as a meta sampler that learns to re-sample training set by meta-learning. [33] proposes a loss that ignores the gradient from samples of large classes for the rare ones, making the training more fair.

A particular group within the cost sensitive training-based methods focuses on optimizing AUC and our method falls into this group. AUC optimization is an ideal choice for class imbalance since AUC is not sensitive to class distributions [7]. [29] proposes a support vector machine (SVM) based loss function that maximizes AUC and demonstrates its effectiveness for the class imbalance. [39] approaches the class imbalance problem from online learning perspective and proposes an AUC optimization-based loss function. [13] proposes a one-pass method for AUC optimization that does not require storing data unlike the previous online methods. Another online AUC optimization method proposed by [37] formulates AUC optimization as a convex-concave saddle point problem. Despite their usefulness, all aforementioned AUC optimization-based methods were applied to linear predictive models, as this allows to simplify the Mann-Whitney statistics [27] for the definition of AUC, and their performance on DNNs is unknown. [32] applies online AUC optimization on a small dataset for breast cancer detection where they also mention that extension to larger datasets may not be feasible. In a very recent work called mini-batch AUC (MBAUC) [14], authors extend AUC optimization to non-linear models with DNNs by optimizing AUC with mini-batches and demonstrate its effectiveness on various datasets.

The proposed constrained optimization method differs from the existing works in that it enforces maximal AUC as a constraint in a way that favors reducing FPR at high TPR and can be used with existing loss functions.

3 Background - Augmented Lagrangian method (ALM)

A generic optimization problem for an objective function $F(\theta)$ subject to the constraints $\mathcal{C}(\theta) = \{c_1(\theta), \dots, c_m(\theta)\}$ can be expressed as [2, 28]:

$$\arg \min_{\theta \in \Theta} F(\theta); \text{ subject to } \mathcal{C}(\theta) \quad (1)$$

Augmented Lagrangian method (ALM) [1], also known as methods of multipliers, converts the constrained optimization problem in Eq. (1) to an unconstrained optimization problem. ALM is proposed to overcome the limitations of two earlier methods called quadratic penalty method and method of Lagrangian multipliers which suffer from training instability and non-convergence due to the difficulty of convexifying loss functions². In ALM, the penalty concept is merged with the primal-dual philosophy of classic Lagrangian function. In such methods, the penalty term is added not to the objective function $F(\theta)$ but rather to its Lagrangian function, thus forming the Augmented Lagrangian Function:

$$\mathcal{L}_\mu(\theta, \lambda) = F(\theta) + \mu \sum_{i=1}^m \|c_i(\theta)\|^2 + \sum_{i=1}^m \lambda_i c_i(\theta) \quad (2)$$

In practice, this method consists in iteratively solving a sequence of problems as:

$$\max_{\lambda^k} \min_{\theta} \mathcal{L}_{\mu^k}(\theta, \lambda^k), \quad \theta \in \Theta \quad (3)$$

Where $\{\lambda^k\}$ is a bounded sequence in \mathcal{R}^m , updated as $\lambda_i^{k+1} = \lambda_i^k + \mu^k c_i(\theta)$. $\{\mu^k\}$ is a positive penalty parameter sequence, with $0 < \mu^k \leq \mu^{k+1}$, $\mu^k \rightarrow \infty$, which may be either pre-selected or generated during the computation according to a defined scheme. In ALM, increasing μ^k indefinitely

²Please consult supplementary material for more details of quadratic penalty method and method of Lagrangian multipliers.

is not necessary as in the quadratic penalty method. Thus, it does not suffer from training instabilities due to the constraint prevailing $F(\theta)$. Furthermore, it does not require convexity assumption as in the method of Lagrange multipliers to ensure convergence [1].

4 Proposed methods

4.1 Proposed constraint for binary classification

Let $F(\theta)$ be a generic loss function that is used to train classification DNNs, $f_\theta(\cdot)$, for binary problems. Let us also define $p \triangleq \{x_1^p, \dots, x_{|p|}^p\}$ and $n \triangleq \{x_1^n, \dots, x_{|n|}^n\}$ as the sets of positive (critical) and negative classes' samples, respectively. Note that we choose p as the minority class in our description, i.e., $|p| < |n|$, and assume that this is a critical class associated with higher risk of making a mistake. We define our constrained optimization problem as follows:

$$\begin{aligned} & \arg \min_{\theta} F(\theta) \\ & \text{subject to } \sum_{k=1}^{|n|} \max \left(0, - \left(f_\theta(x_j^p) - f_\theta(x_k^n) \right) + \delta \right) = 0, \quad j \in \{1, \dots, |p|\}, \end{aligned} \quad (4)$$

where $f_\theta(x)$ indicates output probability of the DNN on input x . Note that the constraint states that the output of the DNN for each critical class' sample should be larger than the outputs of all of the negative samples by a margin δ . Satisfying the constraint would directly ensure maximal AUC [27].

We define the equivalent unconstrained version of Eq. (4) by writing it in the form given in Eq. (2)

$$\mathcal{L}_\mu(\theta, \lambda) = F(\theta) + \frac{\mu \sum_{j=1}^{|p|} q_j^2}{2 \cdot |p| \cdot |n|} + \frac{\sum_{j=1}^{|p|} \lambda_j \cdot q_j}{|p| \cdot |n|} \quad (5)$$

where, $q_j = \sum_{k=1}^{|n|} \max(0, -(f_\theta(x_j^p) - f_\theta(x_k^n)) + \delta)$, μ is the penalty coefficient corresponding to the quadratic penalty term, λ_j is the estimate of Lagrange multiplier corresponding to each positive training sample j , and δ is the margin that we determine using a validation dataset.

The crucial aspect of the above formulation is the asymmetry between positive and negative classes. A constraint is defined for each positive class' sample, thus each positive class' sample gets a separate Lagrange multiplier. This form prioritizes the reduction of FPR at high TPR values as illustrated next.

We use Algorithm 1 to estimate the parameters of a DNN, θ , using the proposed loss function in Eq. 5. The parameters θ are updated with every batch using gradient descent with learning rate α . Concurrently, μ is increased using a multiplicative coefficient ρ only when a chosen metric on validation is not improved, by a margin to avoid training instabilities. The validation metric (*ValMETRIC*) is: 1) Validation AUC for the binary setup; 2) Validation Accuracy for the multi-class version. We update λ in each iteration for each positive sample.

Algorithm 1 ALM for Training DNNs

```

Input:  $\theta^{(0)}, \mu^{(0)}, \lambda_j^{(0)}, \rho$ ;
for  $t = 1, \dots, T$  do
  for each mini-batch of  $x_B$  with size  $B$  do
     $y_B = f(X_B)$ ;
    Calculate  $q_j^{(t)}$ ;  $\triangleright \forall j \in [1, B] \text{ and } y_j = y^+$ 
     $\theta^{(t+1)} \leftarrow \theta^{(t)} - \alpha \cdot \nabla_{\theta} \mathcal{L}_\mu(\theta^{(t)}, \lambda)$ ;
     $\lambda_j^{(t+1)} \leftarrow \lambda_j^{(t)} + \mu^{(t)} \cdot q_j^{(t)}$ ;  $\triangleright \forall j \in [1, B] \text{ and } y_j = y^+$ 
  end for
  if  $ValMETRIC^{(t)} < ValMETRIC^{(t-1)}$  then
     $\mu^{(t+1)} \leftarrow \mu^{(t)} \cdot \rho$ ;
  else
     $\mu^{(t+1)} \leftarrow \mu^{(t)}$ ;
  end if
end for
Return  $\theta^{(t+1)}$ 

```

4.2 Toy example describing our design choice

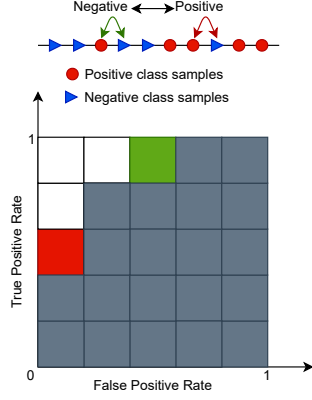


Figure 1: Toy example that illustrates different optimizations, which yield the same improvement in AUC. The one that adds the green box to the AUC however, leads to lower FPRs at the highest TPRs. The ALM given in Eq. (5) prefers adding the green box to improve the AUC rather than the red one.

distances between markers indicate the differences between the outputs of the classifiers for the samples corresponding to the markers. Let us also further assume that all the Lagrange multipliers have the same value. In this case, one can verify that if the optimization swaps the locations of the left most positive sample (red circle marker) and the negative sample to its immediate right (blue triangle marker), the cost due to the constraint in Eq. (5) decreases by $\frac{39\mu\Delta^2}{50} + \frac{3\lambda\Delta}{25}$. Swapping the locations of the right most negative sample and the positive sample to its left decreases the cost due to the constraint by $\frac{19\mu\Delta^2}{50} + \frac{11\lambda\Delta}{25}$ ³. So, from the cost perspective, the optimization should prefer the former swap over the latter, which corresponds to adding the green box to the AUC instead of red box. Therefore, the augmented Lagrangian cost would be decreased further when FPR at the highest TPR is reduced rather than increasing the TPR at the lowest FPR. Instead of defining the constraint for each positive sample in Eq. (5), if we were to define it for each negative sample in the exactly opposite way, i.e., $\sum_{j=1}^{|p|} \max(0, -(f_\theta(x_j^p) - f_\theta(x_k^n)) + \delta) = 0$, $k \in \{1, \dots, |n|\}$, then the situation would be reversed. The optimization would prefer adding the red box over the green box to decrease the cost further. If we were to define a constraint for each positive-negative pair, i.e., $f_\theta(x_j^p) > f_\theta(x_k^n), \forall j$ and k , then adding the red or the green box to improve the AUC would yield exactly the same decrease in the cost.

4.3 Extensions to multi-class classification

The proposed constraint can also be extended to multi-class classification with slight modifications. Let us assume that we have a multi-class classification problem with C classes. In this case, there can be multiple critical and non-critical classes, based on the individual target application. Let us define the corresponding family of sets, i.e., sets of sets, as $P = \{p^1, \dots, p^{|P|}\}$ and $N = \{n^1, \dots, n^{|N|}\}$ where the sets p^i and n^i are as defined in the previous section. Also, note that $|P \cup N| = C$ and $P \cap N = \emptyset$.

A main difference between binary and multi-class classification is the dimension of the output. While $f_\theta(x)$ was a single value for binary classification, in multi-class problem it is a vector with one value for each class. Using the notation for the positive and negative classes, we write the output of the

Recall that our goal with the constraint and the final augmented loss function is to maximize AUC through minimizing FPR for high TPR. The design of the constraint is crucial to achieve this goal. In Fig. 1, we demonstrate this on a toy example. At the top we show 10 data samples and order them with respect to a classifier's output for the samples, i.e., samples on the right are assumed to yield higher output than those on the left. The gray area in the figure below shows the AUC for the toy data samples. Consider two different optimizations to increase the AUC. One adds the red box and the other adds the green box to the gray area. Both optimizations lead to exactly the same AUC improvement, however, only adding the green box reduces FPRs at the highest TPRs.

In the proposed method, we design the constraint to achieve lower FPR at high TPR, such that the optimization can reduce cost more by adding the green box instead of the red box. To see this, let us assume that the distances between all the successive markers in the figure are the same, and we denote this by Δ . Note that the

³Derivations for this toy example and theoretical insights for our design choice are provided in the supplementary material for convenience.

network as $f_\theta(x) = \{f_\theta^{p^1}, \dots, f_\theta^{p^{|P|}}, f_\theta^{n^1}, \dots, f_\theta^{n^{|N|}}\}$. Based on this, we define our first constraint for multi-class classification as

$$q_{cj} = \sum_{i=1}^{|N|} \sum_{k=1}^{|n^i|} \max \left(0, - \left(f_\theta^{p^c}(x_j^{p^c}) - f_\theta^{p^c}(x_k^{n^i}) \right) + \delta \right), \quad c \in \{1, \dots, |P|\}, j \in \{1, \dots, p^c\} \quad (6)$$

where $f_\theta^{p^c}(x)$ indicates the output probability of DNN for the critical class p^c . Note that the constraint in Eq. (6) enforces that the output probability of the DNN for critical classes should be larger for critical class' samples than for samples of other classes.

An alternative definition of the constraint is also possible. The first constraint enforces that critical class' probabilities should be larger for critical class' samples. We can go a step further and add penalty to enforce that non-critical class' probabilities should be smaller for critical samples than the non-critical samples belonging to that class.

$$q_{cj} = \sum_{i=1}^{|N|} \sum_{k=1}^{|n^i|} \max \left(0, - \left(f_\theta^{p^c}(x_j^{p^c}) - f_\theta^{p^c}(x_k^{n^i}) \right) + \delta \right) \\ + \max \left(0, \left(f_\theta^{n^i}(x_j^{p^c}) - f_\theta^{n^i}(x_k^{n^i}) \right) + \delta \right), \quad c \in \{1, \dots, |P|\}, j \in \{1, \dots, p^c\} \quad (7)$$

In this formulation, the penalty does not view all non-critical classes as one but also contributes to increasing classification accuracy in those classes as well, by increasing the gap between the corresponding probability of critical class and non-critical class' samples.

5 Experiments

In this section, we present our experimental evaluations on image-based classification tasks. We perform experiments on three datasets: an in-house MRI medical dataset for prostate cancer and two publicly available computer vision datasets, CIFAR10 and CIFAR100 [19].

In our evaluation, we experiment with different existing loss functions, most of which have been designed to handle class imbalance: classic binary and multi-class cross-entropy (BCE, CE), symmetric margin loss (S-ML) [25], symmetric focal loss (S-FL) [23], asymmetric margin loss (A-ML) and focal loss (A-FL) [22], cost-weighted BCE (WBCE) [38], class-balanced BCE (CB-BCE) and CE (CB-CE) [8], label-distribution-aware margin loss (LDAM) [4]. We first train DNNs for classification using only the loss functions and then using our method, which adds the proposed constraint to the loss function and solves Eq. (5), and we compare the classification performances. In addition, we also compare the proposed method with directly optimizing AUC using the mini-batch AUC (MBAUC) method proposed in [14] for the binary case.

The proposed method is implemented in PyTorch and we run all experiments on a Nvidia GeForce GTX Titan X GPU with 12GB memory.

5.1 Datasets

Prostate MRI dataset consists of 2 distinct cohorts: 1) a group of 300 multiparametric prostate MRI studies used for training and 2) another group of 100 multiparametric prostate MRI studies used for testing the trained DNNs. There is no overlap between the groups. Consent from the each subject is obtained to use the data for research purposes. Two board-certified radiologists with 10 and 7 years of experience in dedicated prostate imaging independently reviewed all examinations of the training set and test set and scored whether Dynamic Contrast Enhanced (DCE) sequences would have been beneficial for cancer diagnosis. After completion of readings, a consensus was reached by the two readers by reviewing all examinations with discrepant decisions. The goal of the binary classification here is to identify subjects who do not require additional DCE imaging for accurate diagnosis, so they can be spared from unnecessary injection and cost and duration of the scanning can be reduced. In our experiments, we randomly split 20% of the training cohort as validation set by keeping the class imbalance consistent across the datasets. In both training and testing cohorts, positive samples represent 13% of all the patients which leads to an inherent 1:8 class ratio.

CIFAR10 and CIFAR100 datasets For CIFAR10, in the binary experiments we randomly select 2 classes among 10 to pose a binary classification problem. Additional experiments with different random selections are in the supplementary material. We use all the available training samples of the selected majority class, while we randomly pick a varying number of training samples for the minority class to obtain different class ratios, up to 1:200. We select 100 samples per class as validation set to determine hyper-parameters. For testing, we use all the available test samples, which consist of 1000 images for each class. For CIFAR100 in the binary setup we select one super-class as majority one, and a sub-class of another super-category as minority one. For training we use all the available 2250 samples of the selected larger class, and we randomly pick a varying number of training samples for the minority class to obtain different class ratios, up to 1:200. We use 50 samples for each original sub-class as validation set to perform the parameters’ search. For testing, we use all the available test samples, which consist of 100 images for each sub-class. For the multi-class experiments, long-tailed versions of CIFAR10 and CIFAR100 are built accordingly to [8, 4] and we consider as the only critical class the smallest one.⁴ Consistently with recent works from the state of the art [8, 4, 30], both validation and test sets are balanced in all the experiments on CIFAR datasets.

5.2 Training details

Network architectures: For the prostate MRI dataset, we use a 3D CNN that consist of cascaded 3D convolution, 3D max-pooling, intermediate ReLu activation functions and Sigmoid in the final output. For the binary CIFAR10 and CIFAR100 datasets, we use ResNet-10, while ResNet-32 [17] is adopted for the multi-class experiments, consistently with [4, 8]. Further training details can be found in the supplementary material.

Ensembling for higher reliability: Model reliability is very crucial when training DNNs. Dealing with small datasets may lead to dataset-dependent results even with the random splits, which could completely hinder objective evaluation. To weaken this phenomenon, we adopt the following ensembling strategy on MRI and for consistency we apply it on the binary CIFAR10 and CIFAR100 as well. Given a dataset and a class ratio, we create 10 random stratified splits of the dataset and train 10 models independently. The larger portions are used for training and the smaller portions for choosing hyper-parameters. During inference, all the models are applied on test samples and predictions are averaged in the logit space before the sigmoid function to yield the final prediction. We apply the ensembling to all the binary models we experiment with. This practice attenuates data dependency and we observed that the final AUC is improved when compared to the average of AUCs of different models, as presented in Table 3 for MRI sequences and in supplementary material for CIFAR10 and CIFAR100.

Hyper-parameters selection: Selection of the best hyper-parameters is crucial both to ensure proper and fair evaluation of the methods and to understand the true performance of any model. To achieve this, we perform grid-search to determine the hyper-parameters that yield the highest AUC for the binary experiments. For the multi-class tests we select the model that achieved the best overall accuracy on the validation set, in order to be consistent with the related works. The test sets in all experiments are not used for hyper-parameter selection. To reduce computational load, we select the common hyper-parameters such as the optimizer, learning rate, and the activation functions in the DNNs based on their performance with BCE loss function for the binary experiments, and consistently with [4] for the multi-class ones. Then, we keep them fixed in all experiments on the same dataset.

Besides the common hyper-parameters, the majority of the existing methods have hyper-parameters that crucially affect their performance. Namely, these hyper-parameters are margin m for S-ML and A-ML, exponent γ for S-FL and A-FL, weight of the cost c for WBCE and β for CB-BCE. We select best values for these hyper-parameters from respective candidate sets that we created based on the information provided in the original papers for each of them.

In the proposed method, there are 4 parameters to be set: $\mu^{(0)}$, $\lambda^{(0)}$, ρ , and δ . Thus, hyperparameters’ search is an important aspect of the proposed method. $\mu^{(0)}$, $\lambda^{(0)}$, and ρ are stemming from ALM and we follow the guideline from [2] when setting them. We initialize all the Lagrangian multipliers $\lambda_i^{(0)}$ to 0. We choose $\mu^{(0)}$ from the set $\{10^{-7}, 10^{-6}, 10^{-5}, 10^{-4}, 10^{-3}\}$, as it is suggested to choose a small value in the beginning and increase it iteratively using the equation $\mu^{(k+1)} = \rho \cdot \mu^{(k)}$. We

⁴Experiments with multiple critical classes are presented in supplementary materials.

choose ρ from the set $\{2, 3\}$ as $\rho > 1$ is suggested. Moreover, we do not increase ρ beyond 4 to avoid potential dominance of the constraint on $F(\theta)$, since ρ is used to increase μ . Once we find the best combination of μ and ρ based on the chosen metrics on the validation set, we fix them and we search for δ as final step. Please see supplementary materials for further details on the hyper-parameters selection.

Once the hyper-parameters for each model are selected, the training is performed and models are applied to the test set to yield the final results, which are described next.

Table 1: Results on binary CIFAR10 for class ratio 1:100 and 1:200.

Dataset	Binary CIFAR10, imb. 100				Binary CIFAR10, imb. 200			
Training method	FPR @ 98% TPR	FPR @ 95% TPR	FPR @ 92% TPR	Test AUC	FPR @ 98% TPR	FPR @ 95% TPR	FPR @ 92% TPR	Test AUC
BCE	56.0	45.0	29.0	91.2	75.0	55.0	40.0	87.3
S-ML	59.0	40.0	26.0	91.7	75.0	54.0	<u>35.0</u>	87.4
S-FL	59.0	40.0	27.0	91.7	78.0	59.0	43.0	85.7
A-ML	54.0	36.0	23.0	92.4	74.0	56.0	39.0	87.4
A-FL	50.0	38.0	24.0	92.3	76.0	59.0	40.0	86.2
CB-BCE	89.0	72.0	59.0	78.0	87.0	74.0	61.0	78.0
W-BCE	69.0	52.0	37.0	87.4	88.0	75.0	62.0	78.3
LDAM	65.0	48.0	34.0	89.0	78.0	63.0	45.0	86.4
MBAUC	86.0	71.0	56.0	74.0	89.0	83.0	69.0	67.9
ALM + BCE	52.0	<u>34.0</u>	<u>21.0</u>	<u>93.1</u>	<u>70.0</u>	54.0	39.0	86.7
ALM + S-ML	50.0	37.0	24.0	92.5	72.0	52.0	39.0	87.9
ALM + S-FL	55.0	39.0	25.0	91.5	74.0	55.0	41.0	86.9
ALM + A-ML	<u>45.0</u>	35.0	23.0	92.8	75.0	74.0	35.0	87.6
ALM + A-FL	<u>49.0</u>	37.0	23.0	92.7	78.0	57.0	37.0	87.0
ALM + CB-BCE	67.0	51.0	36.0	88.1	85.0	69.0	53.0	80.0
ALM + W-BCE	66.0	48.0	31.0	89.3	83.0	69.0	54.0	81.0
ALM + LDAM	60.0	42.0	31.0	91.0	73.0	61.0	43.0	85.6

5.3 Results

We present binary classification results on CIFAR10, CIFAR100, and the in-house medical imaging datasets in Tables 1, 2 and 3, respectively. Bold results indicate which method performs better between the baseline and the same baseline trained with ALM, while the underline highlights the best method. We evaluate the performance of the baselines and the proposed method (ALM) using FPR at maximal levels of TPR (or minimal levels of false negative rate (FNR)) and AUC on the test sets. In the binary experiments, ALM is overall able to consistently improve the performance of almost all the loss functions, with regard to both AUC and FPRs at maximal TPR levels. Even in those cases when AUC is improved to a moderate extent there is still an improvement in FPRs, in accordance with our goal. Moreover, it is noticeable that the higher the TPR, the higher the benefit of applying ALM, which is in accordance with our target applications. In fact, considering that such classifiers in “critical” applications would be operated at high TPR (or low FNR), reduction in FPR in these settings is the effect we desired from the proposed approach. We also observe that ALM improves more when the baseline is performing worse. We calculated Pearson correlation [12] between the average baseline AUC vs average improvement (difference of AUC between baseline and ALM) and obtained -0.85 which indicates a very high negative correlation. Lastly, we also observe in the tables that directly optimizing AUC via MBAUC does not provide the same improvements as using the proposed ALM approach. We present additional binary classification experiments in the supplementary material.

Additionally, we present the quantitative results of multi-class experiments in Table 4. $ALM_{m,1}$ and $ALM_{m,2}$ represent the training with each of the two constraints proposed for the multi-class setting respectively. A bold result for a baseline means that it is able to outperform both the constrained optimisations, otherwise the better constrained strategies are highlighted. As for the binary case,

Table 2: Results on binary CIFAR100 for class ratio 1:100 and 1:200.

Dataset	Binary CIFAR100, imb. 100				Binary CIFAR100, imb. 200			
Training method	FPR @ 98% TPR	FPR @ 95% TPR	FPR @ 90% TPR	Test AUC	FPR @ 98% TPR	FPR @ 95% TPR	FPR @ 90% TPR	Test AUC
BCE	93.0	63.0	47.0	81.8	94.0	77.0	61.0	79.1
S-ML	89.0	65.0	43.0	82.7	95.0	75.0	64.0	79.7
S-FL	89.0	62.0	44.0	82.6	90.0	78.0	50.0	80.1
A-ML	91.0	63.0	44.0	81.8	95.0	75.0	66.0	79.8
A-FL	88.0	63.0	45.0	82.8	91.0	78.0	50.0	80.0
CB-BCE	93.0	75.0	52.0	78.8	93.0	78.0	51.0	78.7
W-BCE	88.0	59.0	41.0	79.7	95.0	63.0	51.0	79.7
LDAM	84.0	70.0	42.0	82.8	80.0	67.0	45.0	82.1
MBAUC	81.0	62.0	41.0	82.3	88.0	63.0	48.0	80.3
ALM + BCE	91.0	49.0	39.0	82.7	87.0	66.0	57.0	80.9
ALM + S-ML	88.0	69.0	41.0	81.7	87.0	73.0	55.0	80.7
ALM + S-FL	88.0	60.0	42.0	81.7	85.0	76.0	50.0	80.8
ALM + A-ML	89.0	55.0	37.0	82.7	92.0	63.0	45.0	81.0
ALM + A-FL	86.0	62.0	40.0	83.2	88.0	76.0	46.0	80.7
ALM + CB-BCE	89.0	59.0	36.0	83.8	85.0	66.0	44.0	81.0
ALM + W-BCE	87.0	53.0	39.0	83.2	79.0	62.0	44.0	81.3
ALM + LDAM	80.0	59.0	40.0	83.2	84.0	61.0	46.0	81.5

underlined results indicate the best method for each metric. Comparison with the other baselines are presented in the supplementary materials. In these experiments, we evaluate the performance by computing the accuracy on the non-critical classes, at various levels of TPR for the critical-class. For this purpose, the first step is to find a threshold on the critical class' logit such that the desired TPR is obtained for the important class. All the test samples whose critical class' logit exceeds the selected threshold are assigned to the important class. The remaining samples that are not assigned to the critical class are then classified based on the highest probability over the non-critical logits. In addition to this metric, we present overall classification accuracy on all classes. The quantitative results demonstrate that both of the multi-class strategies, $ALM_{m,1}$ and $ALM_{m,2}$ improve on the baseline, reducing the error on non-critical classes, at high levels of accuracy on the important class. Moreover, $ALM_{m,2}$ is able to further improve the overall accuracy by a larger margin in almost all the experiments thanks to the additional term in the constraint.

6 Conclusion

In this paper, we pose the training of a DNN for binary classification under class imbalance as a constrained optimization problem and propose a novel constraint that can be used with existing loss functions. The proposed constraint is designed to maximize the AUC, but in an asymmetric way to favor the reduction of FPR at high TPR (or low FNR). Then, we transfer the constrained problem to its dual unconstrained optimization problem using an Augmented Lagrangian method (ALM) [2] which we optimize using stochastic gradient descent. Additionally, we presented two possible extensions of the proposed constraint for multi-class classification problems.

We perform an extensive evaluation of the proposed constraints for binary and multi-class image classification problems on both computer vision and medical imaging datasets. We compare the performance of the proposed constraints with different baselines by simulating different class imbalance ratio. The quantitative results demonstrate that the proposed constraints improve the performance of the baselines in the majority of the cases in both binary and multi-class classification experiments.

Table 3: Results on in-house MRI dataset.

Method	FPR @0 FN	FPR @1 FN	Avg AUC	AUC ens.
BCE	80.0	80.0	65.4±9.0	70.9
S-ML	81.0	77.0	67.3±7.0	71.5
S-FL	77.0	38.0	71.7±10.0	80.3
A-ML	77.0	73.0	68.0±9.0	74.2
A-FL	66.0	38.0	67.7±8.0	80.1
CB-BCE	100.0	34.0	72.0±5.0	77.7
W-BCE	56.0	42.0	68.8±6.0	80.5
LDAM	100.0	75.0	62.0±9.0	66.4
MBAUC	61.2	33.0	71.2±11.0	82.4
ALM + BCE	54.0	38.0	76.8±9.0	85.4
ALM + S-ML	81.0	33.0	72.5±9.0	80.3
ALM + S-FL	53.0	26.0	72.5±10.0	84.2
ALM + A-ML	72.0	53.0	67.2±5.0	76.4
ALM + A-FL	62.0	46.0	74.7±7.0	81.5
ALM + CB-BCE	86.0	34.0	73.0±9.0	79.5
ALM + W-BCE	59.0	40.0	72.4±6.0	81.4
ALM + LDAM	59.0	53.0	66.5±8.5	77.0

Table 4: Results on long-tailed CIFAR10 for class imbalance 1:100 and 1:200. The Table shows the error on all the non-important classes, after setting a threshold on the important class’ logit to obtain 80, 90% TPR.

Dataset	Long-tailed CIFAR10, imb. 100			Long-tailed CIFAR10, imb. 200		
Training method	Error @ 80% TPR	Error @ 90% TPR	Overall Accuracy	Error @ 80% TPR	Error @ 90% TPR	Overall Accuracy
CE	29.80	34.67	70.35	37.81	42.37	64.03
FL	32.21	36.47	69.20	38.50	42.21	62.90
CB-BCE	31.04	33.44	72.90	35.11	39.13	65.77
LDAM	26.57	29.86	71.80	34.41	45.72	65.87
ALM _{m,1} + CE	28.89	33.93	70.90	36.14	39.90	65.13
ALM _{m,1} + FL	29.59	34.94	69.74	36.87	41.87	64.23
ALM _{m,1} + CB-CE	27.89	30.27	72.10	33.09	35.44	65.34
ALM _{m,1} + LDAM	25.73	28.52	72.86	31.94	37.41	65.65
ALM _{m,2} + CE	29.53	34.09	71.30	35.10	39.19	64.35
ALM _{m,2} + FL	30.50	35.63	69.47	36.27	40.43	64.43
ALM _{m,2} + CB-CE	27.84	31.97	72.09	33.72	36.86	66.04
ALM _{m,2} + LDAM	24.76	28.91	73.32	31.02	36.09	67.41

7 Acknowledgments

The presented work was partly funding by: 1. Clinical Research Priority Program Grant on Artificial Intelligence in Oncological Imaging Network, University of Zurich and 2. Personalized Health and Related Technologies (PHRT), project number 222, ETH domain.

References

- [1] Bertsekas, D.P.: Multiplier methods: A survey. *Automatica* **12**(2), 133 – 145 (1976). [https://doi.org/https://doi.org/10.1016/0005-1098\(76\)90077-7](https://doi.org/https://doi.org/10.1016/0005-1098(76)90077-7), <http://www.sciencedirect.com/science/article/pii/S0005109876900777>
- [2] Bertsekas, D.: *Nonlinear Programming*. Athena Scientific (1999)
- [3] Buda, M., Maki, A., Mazurowski, M.A.: A systematic study of the class imbalance problem in convolutional neural networks. *Neural Networks* **106**, 249 – 259 (2018). <https://doi.org/https://doi.org/10.1016/j.neunet.2018.07.011>, <http://www.sciencedirect.com/science/article/pii/S0893608018302107>
- [4] Cao, K., Wei, C., Gaidon, A., Arechiga, N., Ma, T.: Learning imbalanced datasets with label-distribution-aware margin loss. In: Wallach, H., Larochelle, H., Beygelzimer, A., d'Alché-Buc, F., Fox, E., Garnett, R. (eds.) *Advances in Neural Information Processing Systems*. vol. 32. Curran Associates, Inc. (2019), <https://proceedings.neurips.cc/paper/2019/file/621461af90cadfdaf0e8d4cc25129f91-Paper.pdf>
- [5] Chan, R., Rottmann, M., Hüger, F., Schlicht, P., Gottschalk, H.: Application of decision rules for handling class imbalance in semantic segmentation. *arXiv preprint arXiv:1901.08394* (2019)
- [6] Chawla, N.V., Bowyer, K.W., Hall, L.O., Kegelmeyer, W.P.: Smote: Synthetic minority over-sampling technique. *J. Artif. Int. Res.* **16**(1), 321–357 (Jun 2002)
- [7] Cortes, C., Mohri, M.: Auc optimization vs. error rate minimization. *Advances in neural information processing systems* **16**(16), 313–320 (2004)
- [8] Cui, Y., Jia, M., Lin, T.Y., Song, Y., Belongie, S.: Class-balanced loss based on effective number of samples. In: *Proceedings of the IEEE/CVF Conference on Computer Vision and Pattern Recognition*. pp. 9268–9277 (2019)
- [9] DeLong, E., DeLong, D., Clarke-Pearson, D.: Comparing the areas under two or more correlated receiver operating characteristic curves: a nonparametric approach. *Biometrics* **44**(3), 837–845 (September 1988). <https://doi.org/10.2307/2531595>
- [10] Djavan, B., Zlotta, A., Remzi, M., Ghawidel, K., Basharkhah, A., Schulman, C., Marberger, M.: Optimal predictors of prostate cancer on repeat prostate biopsy: a prospective study of 1,051 men. *The Journal of urology* **163** 4, 1144–8; discussion 1148–9 (2000)
- [11] Drummond, C., Holte, R.C., et al.: C4. 5, class imbalance, and cost sensitivity: why under-sampling beats over-sampling. In: *Workshop on learning from imbalanced datasets II*. vol. 11, pp. 1–8. Citeseer (2003)
- [12] Freedman, D., Pisani, R., Purves, R.: *Statistics (international student edition)*. Pisani, R. Purves, 4th edn. WW Norton & Company, New York (2007)
- [13] Gao, W., Jin, R., Zhu, S., Zhou, Z.H.: One-pass auc optimization. In: *International conference on machine learning*. pp. 906–914. PMLR (2013)
- [14] Gultekin, S., Saha, A., Ratnaparkhi, A., Paisley, J.: Mba: mini-batch auc optimization. *IEEE transactions on neural networks and learning systems* **31**(12), 5561–5574 (2020)
- [15] Haibo He, Yang Bai, Garcia, E.A., Shutao Li: Adasyn: Adaptive synthetic sampling approach for imbalanced learning. In: *2008 IEEE International Joint Conference on Neural Networks (IEEE World Congress on Computational Intelligence)*. pp. 1322–1328 (2008). <https://doi.org/10.1109/IJCNN.2008.4633969>
- [16] He, H., Garcia, E.: Learning from imbalanced data. *Knowledge and Data Engineering, IEEE Transactions on* **21**, 1263 – 1284 (10 2009). <https://doi.org/10.1109/TKDE.2008.239>
- [17] He, K., Zhang, X., Ren, S., Sun, J.: Deep residual learning for image recognition. *2016 IEEE Conference on Computer Vision and Pattern Recognition (CVPR)* pp. 770–778 (2016)

- [18] Huang, C., Li, Y., Loy, C.C., Tang, X.: Learning deep representation for imbalanced classification. In: Proceedings of the IEEE conference on computer vision and pattern recognition. pp. 5375–5384 (2016)
- [19] Krizhevsky, A., Hinton, G., et al.: Learning multiple layers of features from tiny images (2009)
- [20] Lakshminarayanan, B., Pritzel, A., Blundell, C.: Simple and scalable predictive uncertainty estimation using deep ensembles (2017)
- [21] Lawrence, S., Burns, I., Back, A., Tsoi, A., Giles, C.L.: Neural network classification and prior class probabilities. In: Neural Networks: Tricks of the Trade (1996)
- [22] Li, Z., Kamnitsas, K., Glocker, B.: Overfitting of neural nets under class imbalance: Analysis and improvements for segmentation. In: International Conference on Medical Image Computing and Computer-Assisted Intervention. pp. 402–410. Springer (2019)
- [23] Lin, T.Y., Goyal, P., Girshick, R., He, K., Dollár, P.: Focal loss for dense object detection. In: Proceedings of the IEEE international conference on computer vision. pp. 2980–2988 (2017)
- [24] Litjens, G., Kooi, T., Bejnordi, B.E., Setio, A.A.A., Ciompi, F., Ghafoorian, M., van der Laak, J.A., van Ginneken, B., Sánchez, C.I.: A survey on deep learning in medical image analysis. *Medical Image Analysis* **42**, 60–88 (Dec 2017). <https://doi.org/10.1016/j.media.2017.07.005>, <http://dx.doi.org/10.1016/j.media.2017.07.005>
- [25] Liu, W., Wen, Y., Yu, Z., Yang, M.: Large-margin softmax loss for convolutional neural networks. In: ICML. vol. 2, p. 7 (2016)
- [26] Liu, Z., Wei, P., Jiang, J., Cao, W., Bian, J., Chang, Y.: Mesa: Boost ensemble imbalanced learning with meta-sampler. In: Conference on Neural Information Processing Systems (2020)
- [27] Mann, H.B., Whitney, D.R.: On a test of whether one of two random variables is stochastically larger than the other. *The annals of mathematical statistics* pp. 50–60 (1947)
- [28] Nocedal, J., Wright, S.J.: Numerical Optimization. Springer, New York, NY, USA, second edn. (2006)
- [29] Rakotomamonjy, A.: Optimizing area under roc curve with svms. In: ROCAI. pp. 71–80 (2004)
- [30] Ren, J., Yu, C., Sheng, S., Ma, X., Zhao, H., Yi, S., Li, H.: Balanced meta-softmax for long-tailed visual recognition. In: Proceedings of Neural Information Processing Systems(NeurIPS) (Dec 2020)
- [31] Shamsolmoali, P., Zareapoor, M., Shen, L., Sadka, A.H., Yang, J.: Imbalanced data learning by minority class augmentation using capsule adversarial networks. *Neurocomputing* (2020)
- [32] Sulam, J., Ben-Ari, R., Kisilev, P.: Maximizing auc with deep learning for classification of imbalanced mammogram datasets. In: VCBM. pp. 131–135 (2017)
- [33] Tan, J., Wang, C., Li, B., Li, Q., Ouyang, W., Yin, C., Yan, J.: Equalization loss for long-tailed object recognition. In: Proceedings of the IEEE/CVF Conference on Computer Vision and Pattern Recognition (CVPR) (June 2020)
- [34] Thai-Nghe, N., Gantner, Z., Schmidt-Thieme, L.: Cost-sensitive learning methods for imbalanced data. In: The 2010 International joint conference on neural networks (IJCNN). pp. 1–8. IEEE (2010)
- [35] Tian, J., Liu, Y.C., Glaser, N., Hsu, Y.C., Kira, Z.: Posterior re-calibration for imbalanced datasets (2020)
- [36] Wang, S., Liu, W., Wu, J., Cao, L., Meng, Q., Kennedy, P.J.: Training deep neural networks on imbalanced data sets. In: 2016 international joint conference on neural networks (IJCNN). pp. 4368–4374. IEEE (2016)
- [37] Ying, Y., Wen, L., Lyu, S.: Stochastic online auc maximization. In: NIPS. pp. 451–459 (2016)

- [38] Zadrozny, B., Langford, J., Abe, N.: Cost-sensitive learning by cost-proportionate example weighting. In: Third IEEE international conference on data mining. pp. 435–442. IEEE (2003)
- [39] Zhao, P., Hoi, S.C., Jin, R., YANG, T.: Online auc maximization (2011)

A Additional Experiments

A.1 Additional experiments on binary classification

In Table 5, we provide results for the additional class ratio on CIFAR10 of 1:50. The results demonstrate the effectiveness of the proposed method even at a lower class imbalance and show consistency with the results at higher imbalance presented in the main paper.

Table 5: Results on binary CIFAR10 for the same classes as in the main paper, at 1:50 class ratio.

Dataset	Binary CIFAR10, imb. 50			
Training method	FPR @ 98% TPR	FPR @ 95% TPR	FPR @ 90% TPR	Test AUC
BCE	34.1	21.3	11.1	96.05
S-ML	31.6	18.0	9.2	96.48
S-FL	31.9	18.0	10.1	96.20
A-ML	28.4	17.0	10.6	96.29
A-FL	36.1	20.0	11.3	95.86
CB-BCE	84.6	72.3	55.4	79.73
W-BCE	36.9	22.5	12.8	95.29
LDAM	45.2	21.0	8.9	95.65
MBAUC	75.0	60.5	47.0	82.47
ALM + BCE	30.7	17.4	7.9	96.49
ALM + S-ML	31.1	17.0	8.9	96.41
ALM + S-FL	28.4	17.9	11.3	96.15
ALM + A-ML	28.7	16.1	9.2	96.40
ALM + A-FL	32.7	17.1	9.3	96.2
ALM + CB-BCE	52.9	35.5	25.8	91.78
ALM + W-BCE	32.4	18.4	11.2	95.87
ALM + LDAM	33.8	14.2	8.1	96.61

In Table 6, in addition to the experiments with 2 randomly selected classes of CIFAR10, we provide results for other two randomly selected classes. In this experiment, we present FPR results at higher TPRs compared to the results in the main paper because at lower thresholds, both baselines and ALM already perform quite well.

A.2 Comparison with additional baselines for multi-class experiments on long-tailed CIFAR100

Due to space reason, in the main paper we report the comparison with only four methods for the multi-class experiments. In Table 7 we show the results on long-tailed CIFAR10 for other three baselines from the SoA. The results are consistent with the main paper where ALM improves the baselines in majority of the cases.

A.3 Multi-class experiments on long-tailed CIFAR100

Table 8 shows the results on long-tailed CIFAR100, for class ratios 1:20 and 1:50. We test on a lower imbalance ratio on CIFAR100, compared to CIFAR10, because there are only 500 samples per class in the original CIFAR100 and using higher ratios would mean having only a few critical class samples, which provides very little information.

A.4 Experiments with multiple critical classes

So far, we have performed experiments for the cases where there is only a single critical class. However, in practice, there may be multiple critical classes where missing a sample has a high cost. In Table 9 we present results when there are two critical, under-represented classes. In this case, we

Table 6: Results on binary CIFAR10 for class ratio 1:100 and 1:200 for two randomly selected classes different than the ones presented in the main paper.

Dataset	Binary CIFAR10, imb. 100				Binary CIFAR10, imb. 200			
Training method	FPR @ 100% TPR	FPR @ 99% TPR	FPR @ 96% TPR	Test AUC	FPR @ 100% TPR	FPR @ 99% TPR	FPR @ 96% TPR	Test AUC
BCE	78.0	30.0	13.0	97.9	85.0	43.0	26.0	95.9
S-ML	78.0	34.0	14.0	97.9	98.0	62.0	25.0	95.2
S-FL	84.0	35.0	12.0	98.0	77.0	45.0	24.0	96.1
A-ML	91.0	34.0	14.0	97.9	85.0	52.0	27.0	95.7
A-FL	84.0	39.0	13.0	98.0	91.0	54.0	22.0	96.0
CB-BCE	81.0	59.0	36.0	92.6	81.0	57.0	35.0	92.2
W-BCE	87.0	55.0	24.0	95.0	97.0	68.0	44.0	91.6
LDAM	80.0	33.0	14.0	97.9	78.0	51.0	26.0	95.8
MBAUC	88.0	54.0	34.0	90.9	85.0	56.0	42.0	89.4
ALM + BCE	58.0	34.0	10.0	98.2	82.0	39.0	24.0	96.3
ALM + S-ML	72.0	34.0	12.0	98.0	92.0	52.0	24.0	96.1
ALM + S-FL	69.0	30.0	13.0	98.1	72.0	49.0	24.0	96.0
ALM + A-ML	78.0	25.0	11.0	98.2	83.0	54.0	26.0	96.0
ALM + A-FL	75.0	33.0	13.0	98.2	72.0	47.0	21.0	96.4
ALM + CB-BCE	76.0	49.0	26.0	95.3	70.0	47.0	27.0	95.1
ALM + W-BCE	82.0	54.0	25.0	95.3	86.0	61.0	42.0	91.0
ALM + LDAM	71.0	25.0	11.0	98.4	65.0	46.0	29.0	94.8

Table 7: Results on long-tailed CIFAR10 for class imbalance 1:100 and 1:200, comparing to other baselines. The table shows the error on all the non-important classes, after setting a threshold on the important class’s logit to obtain 80, 90% TPR as well as the overall accuracy.

Dataset	Long-tailed CIFAR10, imb. 100			Long-tailed CIFAR10, imb. 200		
Training method	Error @ 80% TPR	Error @ 90% TPR	Overall Accuracy	Error @ 80% TPR	Error @ 90% TPR	Overall Accuracy
S-LM	30.69	35.09	71.94	38.17	41.74	64.49
A-LM	31.56	37.12	69.51	36.41	40.75	64.38
A-FL	29.80	65.33	70.35	36.12	41.26	64.12
ALM _{m,1} + S-LM	29.90	33.70	71.61	36.37	38.96	64.20
ALM _{m,1} + A-LM	30.07	35.49	70.32	35.23	39.18	64.14
ALM _{m,1} + A-FL	28.97	34.13	70.20	35.04	38.63	64.71
ALM _{m,2} + S-LM	29.62	33.92	70.85	37.93	40.74	64.81
ALM _{m,2} + A-LM	29.24	34.73	71.69	34.96	38.65	65.08
ALM _{m,2} + A-FL	28.70	32.73	71.27	34.59	39.70	64.52

report the accuracy of each of the two important classes along with the accuracy on the non-critical ones. Overall, the proposed method is able to improve in almost all the cases the accuracy on the important classes, keeping a comparable accuracy in all the non-critical ones.

A.5 Additional categories of Related Work

In the main paper we present related work about learning with class imbalance belonging to the cost sensitive training-based methods category. We decided to focus on this first because the presented method belongs to this category, and consequently it has been the focus of the discussion, secondly because of space reasons. In this Section we present the other two main categories of techniques that aim to address this aspect: sampling-based and classifier-based methods.

Table 8: Results on long-tailed CIFAR100 for class imbalance 1:20 and 1:50. The table shows the error on all the non-important classes, after setting a threshold on the important class’ logit to obtain 80, 90% TPR as well as the overall accuracy.

Dataset	CIFAR100, imb. 20			CIFAR10, imb. 50		
Training method	Error @ 80% TPR	Error @ 90% TPR	Overall Accuracy	Error @ 80% TPR	Error @ 90% TPR	Overall Accuracy
CE	92.00	92.55	49.46	93.31	94.56	43.17
FL	91.96	92.69	49.73	92.33	93.94	42.96
CB-BCE	92.20	93.27	50.02	93.44	94.97	42.18
LDAM	92.01	92.57	49.60	93.83	94.93	44.29
ALM _{m,1} + CE	91.39	91.87	50.82	92.60	93.50	43.45
ALM _{m,1} + FL	91.40	91.95	50.27	92.25	92.99	43.52
ALM _{m,1} + CB-CE	91.44	92.09	51.36	92.84	94.28	42.47
ALM _{m,1} + LDAM	91.40	92.18	50.08	93.31	94.43	43.95
ALM _{m,2} + CE	91.74	92.05	50.47	92.69	94.40	43.52
ALM _{m,2} + FL	91.67	91.99	49.88	92.10	93.00	43.56
ALM _{m,2} + CB-CE	91.75	92.60	50.73	92.66	93.48	42.43
ALM _{m,2} + LDAM	91.65	92.38	50.10	92.61	93.22	43.74

Table 9: Results on long-tailed CIFAR10 for class imbalance 1:100 and 1:200, when the two smallest classes are identified as critical and under-represented. The table shows the accuracy on the two critical classes, the smallest identified as Class 1 and the other named Class 2, as well the accuracy over all the non-critical ones.

Dataset	CIFAR10, imb. 100			CIFAR10, imb. 200		
Training method	Acc. Critical Class 1	Acc. Critical Class 2	Acc. Other Classes	Acc. Critical Class 1	Acc. Critical Class 2	Acc. Other Classes
CE	38.9	48.0	77.1	23.1	32.0	73.0
FL	37.5	37.0	76.2	22.7	24.5	72.7
CB-BCE	50.6	58.6	77.0	30.6	37.3	73.7
LDAM	48.9	44.5	78.1	33.1	30.6	74.4
ALM _{m,1} + CE	43.0	50.0	77.0	32.0	29.0	73.7
ALM _{m,1} + FL	41.0	41.6	76.6	25.8	31.5	72.6
ALM _{m,1} + CB-CE	53.9	51.2	77.2	38.3	39.7	74.0
ALM _{m,1} + LDAM	50.3	44.5	78.0	35.2	31.5	74.4
ALM _{m,2} + CE	41.1	54.1	77.3	30.1	32.1	73.5
ALM _{m,2} + FL	38.9	48.3	76.8	28.1	26.6	72.8
ALM _{m,2} + CB-CE	53.6	56.7	76.6	33.8	45.3	73.1
ALM _{m,2} + LDAM	50.0	47.1	78.0	34.5	30.4	74.6

Sampling-based methods: Methods in this group aim to deal with the data imbalance problem by generating a balanced distribution through getting more samples from the minority class or less samples from the majority class. A simple approach of replicating a certain number of minority class’ instances can lead to models that are over-fitting to the over-sampled instances. [6] proposes to generate novel minority class’ samples by interpolating the neighboring data points. [15] extends [6] by proposing a way to estimate the number of minority class’ samples to be synthesized. [11] approaches the problem from the opposite perspective and randomly under-sample majority class instances instead of synthesizing new data for the minority class. Despite the fact that losing valuable information for the majority class, [11] reports that it leads to better results compared to the former approaches. Although, these earlier sampling-based methods are useful for the low dimensional data, they suffer from issues in higher dimensions, e.g. images, since interpolation does not lead to

realistic samples. Moreover, they still suffer from generalization difficulties [16]. [31] proposes to use adversarial training with capsule networks to generate more realistic samples for the minority classes, and demonstrate its effectiveness for class imbalance. More recently, [26] proposes a method which adaptively samples a subset from the training set in each iteration to train multiple classifiers which are then ensembled for prediction.

Classifier-based methods: Methods from this category operate in test time and are mostly based on thresholding and scaling the output class probabilities. One common approach is to divide the output for each class by their prior probabilities which shown to be effective to handle class imbalance in both classification [21, 3] and semantic segmentation [5]. In a recent work, [35] argue that the previous methods from this family suffer from diminished overall accuracy despite the improved detection on minority classes. They mitigate this problem by proposing a method re-balancing the posterior in test-time.

B Background = Augmented Lagrangian Method

The Augmented Lagrangian Method is based on two previously developed techniques, which are combined together into ALM, overcoming the respective drawbacks.

A generic optimization problem for an objective function $F(\theta)$ subject to the constraints $\mathcal{C}(\theta) = \{c_1(\theta), \dots, c_m(\theta)\}$ can be expressed as [2, 28]:

$$\begin{aligned} & \arg \min_{\theta} F(\theta) \\ & \text{subject to } \mathcal{C}(\theta), \quad \theta \in \Theta \end{aligned} \quad (8)$$

One of the earlier methods, quadratic penalty method [1], converts the constrained optimization problem in Eq. (8) to an unconstrained optimization problem by adding the constraint to the objective function as a quadratic penalty term:

$$\arg \min_{\theta \in \Theta} F(\theta) + \mu \sum_{i=1}^m \|c_i(\theta)\|^2 \quad (9)$$

where μ is a positive parameter which controls the contribution of the penalty term to the overall loss function. Increasing μ indefinitely over the iterations is necessary to convexify the loss and ensure convergence. However, as μ increases, the penalty term prevails $F(\theta)$, which makes training unstable [1].

The method of Lagrange multipliers converts Eq. (1) into the unconstrained optimization problem by adding the constraints to the objective function as follows:

$$\mathcal{L}(\theta, \lambda) = F(\theta) + \sum_{i=1}^m \lambda_i c_i(\theta) \quad (10)$$

where λ are called as Lagrange multipliers. The method of Lagrange multipliers deals with the instability of quadratic penalty method, however, it requires the objective function to be convex which is a drawback.

Augmented Lagrangian Methods overcome the limitations of the above-mentioned two approaches. Here, the penalty concept is merged with the primal-dual philosophy of classic Lagrangian function, as explained in the main paper.

C Theoretical Insights

In this Section we derive a few theoretical insights to motivate the choice of our constraint with the aid of an example. Let us consider the situation depicted in Figure 2 of a binary classification task, where the NN is correctly ordering all the samples, except for one mistake for each class. This case can be then generalised for a larger number of mistakes. For simplicity, let us consider Δ as the distance between all adjacent pairs of correct samples, Δ_N as distance between the misclassified negative sample and the rightmost positive sample and finally Δ_P as the distance between the misclassified positive sample and the leftmost negative sample. Let M and N be the number of positive and negative

examples, respectively and $M \leq N$, i.e. positive class is smaller (or equal) than negative class, which corresponds to the setup of interest. Our goal is to show that: 1) the proposed constraint encourages the loss to reduce the error on the positive sample (i.e. improving TPR) instead of the negative one; 2) the other asymmetric variant (i.e. $\sum_{j=1}^M \max(0, -(f_\theta(x_j^+) - f_\theta(x_k^-)) + \delta) = 0$, $k \in \{1, \dots, N\}$) wouldn't have been as effective as the chosen one.

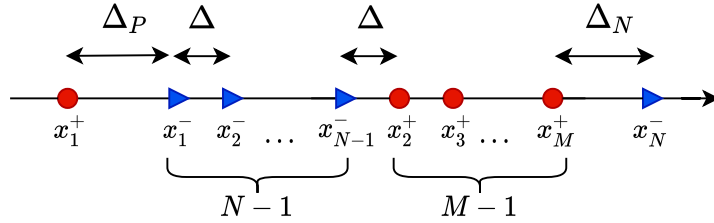


Figure 2: Auxiliary example to explain the motivations behind the chosen constraint. All the correctly ranked samples are separated by a distance Δ , while the errors amount to Δ_N and Δ_P , for the negative and positive errors respectively.

Accordingly to our solution the update of multiplier for each positive training sample is:

$$\begin{aligned} \lambda_1 &= \lambda + \mu \left(\sum_{k=0}^{N-2} \Delta_P + k\Delta \right) \\ \lambda_{M-j} &= \lambda + \mu(\Delta_N + \Delta j) \quad j = 0, \dots, M-2 \end{aligned} \tag{11}$$

Consequently, the loss terms corresponding to ALM are:

$$\begin{aligned}
\tilde{L}_\mu(\theta, \lambda) &= \frac{\mu}{2} \left[\left(\sum_{k=0}^{N-2} \Delta_P + k\Delta \right)^2 + \sum_{j=0}^{M-2} (\Delta_N + j\Delta)^2 \right] \\
&+ \left[\left(\lambda + \mu \sum_{k=0}^{N-2} \Delta_P + k\Delta \right) \left(\sum_{k=0}^{N-2} \Delta_P + k\Delta \right) + \sum_{j=0}^{M-2} (\lambda + \mu(\Delta_N + j\Delta))(\Delta_N + j\Delta) \right] = \\
&= \frac{3\mu}{2} \left(\sum_{k=0}^{N-2} \Delta_P + k\Delta \right)^2 + \lambda \sum_{k=0}^{N-2} (\Delta_P + k\Delta) + \frac{3\mu}{2} \sum_{j=0}^{M-2} (\Delta_N + j\Delta)^2 + \lambda \sum_{j=0}^{M-2} (\Delta_N + j\Delta) = \\
&= \frac{3\lambda}{2} \left[\Delta_P(N-1) + \Delta \frac{(N-1)(N-2)}{2} \right]^2 + \Delta_P \lambda(N-1) + \lambda \Delta \frac{(N-1)(N-2)}{2} \\
&+ \frac{3\mu}{2} \left[\Delta_N^2(M-1) + \Delta^2 \frac{(2M-3)(M-1)(M-2)}{6} + \Delta_N 2\Delta \frac{(M-1)(M-2)}{2} \right] \\
&+ \Delta_N \lambda(M-1) + \lambda \Delta \frac{(M-1)(M-2)}{2} = \\
&= \frac{3\mu}{2} \left[\Delta_P^2(N-1)^2 + \Delta_N^2(M-1) \right] \\
&+ \Delta_P \left[\frac{3}{2} \mu \Delta(N-1)^2(N-2) + \lambda(N-1) \right] + \Delta_N \left[\frac{3}{2} \mu \Delta(M-1)(M-2) + \lambda(M-1) \right] \\
&+ \frac{3}{2} \mu \Delta^2 \left(\frac{((N-1)(N-2))^2}{4} + \frac{(2M-3)(M-1)(M-2)}{6} \right) \\
&+ \lambda \Delta \left(\frac{(N-1)(N-2)}{2} + \frac{(M-1)(M-2)}{2} \right)
\end{aligned} \tag{12}$$

Insight 1: It is evident from the final result of Equation 12 that, given $M \leq N$ (in our experiments the inequality is strict) and given the same error ($\Delta_P = \Delta_N$), the contribution to the loss function from the misclassified positive sample is larger than the contribution of the negative one. This means that we are putting more emphasis on errors in the smaller class, even when the entity of the mistake is the same for both classes. As a consequence, removing the error Δ_P would reduce the loss more than removing the error Δ_N . Moreover, it is clear that this difference in error weighing increases with the level of imbalance between the classes. This results not only from the different number of samples per class, but also from the presence of higher powers in the coefficients of Δ_P in Equation 12, i.e. $(N-1)^2$ in both the terms with Δ_P . Clearly, this consideration holds even more in the case where $\Delta_P \geq \Delta_N$, as the difference is further enforced.

Differently, if $\Delta_N \geq \Delta_P$ it is not always guaranteed that removing the error Δ_P reduces the loss more than removing the error Δ_N . Fixing Δ_P , M , and N (with $M \leq N$), Δ_N may be increased such that its contribution is higher than the one from the positive sample. In order to visually understand this, Figure 3 shows two possible contributions to the loss from the positive (L_P) and negative (L_N) errors. At the same $\Delta_P = \Delta_N = \Delta_E$ or at $\Delta_P \geq \Delta_N$ the contribution of the mistake on the positive example is higher. However, this does not hold anymore when, fixed Δ_P , Δ_N exceeds a certain $\Delta_P + \Delta_{diff,lim}$. In this situation, when $\Delta_N \geq \Delta_P + \Delta_{diff,lim}$, the condition $L_P \geq L_N$ does not hold anymore.

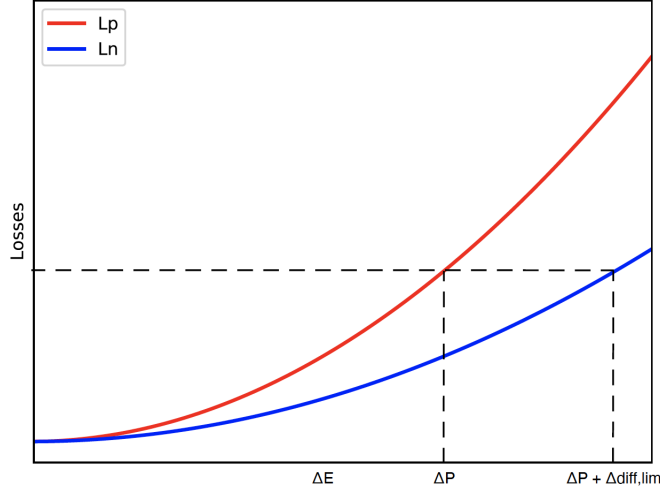


Figure 3: Trend of the two contributions of positive and negative errors.

In order to find $\Delta_{diff,lim}$ it is necessary that the following equation for Δ_{diff} is satisfied:

$$\begin{aligned} \Delta_P^2(N-1)^2 + \Delta_P \left[\frac{3}{2}\mu\Delta(N-1)^2(N-2) + \lambda(N-1) \right] = \\ (\Delta_P + \Delta_{diff})^2(M-1) + (\Delta_P + \Delta_{diff}) \left[\frac{3}{2}\mu\Delta(M-1)(M-2) + \lambda(M-1) \right] \end{aligned} \quad (13)$$

For readability Equation 13 may be rewritten as:

$$\Delta_P^2 a + \Delta_P b = (\Delta_P + \Delta_{diff})^2 c + (\Delta_P + \Delta_{diff}) d \quad (14)$$

Which leads to:

$$\begin{aligned} c\Delta_{diff}^2 + (2\Delta_P c + d)\Delta_{diff} + (\Delta_P^2(c-a) + \Delta_P(d-b)) = 0 \\ \Delta_{diff,lim} = \frac{-(2\Delta_P c + d) + \sqrt{(2\Delta_P c + d)^2 - 4c(\Delta_P^2(c-a) + \Delta_P(d-b))}}{2c} \end{aligned} \quad (15)$$

We take only the positive square root as $\Delta_{diff,lim}$ has to be positive and the discriminant of the equation is positive for $N \geq M$. A few considerations can be drawn about how $\Delta_{diff,lim}$ varies. The higher the class imbalance, the higher $\Delta_{diff,lim}$ becomes (as this affects the discriminant in the equation). Similarly, the larger the fixed Δ_P , the larger $\Delta_{diff,lim}$.

However in practice, being NNs typically biased towards majority class, it is likely that this last case of $\Delta_P < \Delta_N$ rarely occurs.

Insight 2: Let us now show that choosing the symmetrically opposite constraint would have been less efficient than the proposed method for our purpose. Accordingly to the alternative version of the constraint, the Lagrange multipliers would have been updated as follows:

$$\begin{aligned} \lambda_{k+1} &= \lambda + \mu(\Delta_N + \Delta_k) \quad k = 0, \dots, N-2 \\ \lambda_N &= \lambda + \mu \left(\sum_{j=0}^{M-2} \Delta_N + j\Delta \right) \end{aligned} \quad (16)$$

And the loss function would have become:

$$\begin{aligned}
\tilde{L}_\mu(\theta, \lambda) &= \frac{\mu}{2} \left[\left(\sum_{j=0}^{M-2} \Delta_N + j\Delta \right)^2 + \sum_{k=0}^{N-2} (\Delta_P + j\Delta)^2 \right] \\
&+ \left[\left(\lambda + \mu \sum_{j=0}^{M-2} \Delta_N + j\Delta \right) \left(\sum_{j=0}^{M-2} \Delta_N + j\Delta \right) + \sum_{k=0}^{N-2} (\lambda + \mu(\Delta_P + k\Delta))(\Delta_P + k\Delta) \right] = \\
&= \frac{3\mu}{2} \left(\sum_{j=0}^{M-2} \Delta_N + j\Delta \right)^2 + \lambda \sum_{k=0}^{N-2} (\Delta_P + k\Delta) + \frac{3\mu}{2} \sum_{k=0}^{N-2} (\Delta_P + k\Delta)^2 + \lambda \sum_{j=0}^{M-2} (\Delta_N + j\Delta) = \\
&= \dots = \\
&= \frac{3\mu}{2} \left[\Delta_P^2(N-1) + \Delta_N^2(M-1)^2 \right] \\
&+ \Delta_P \left[\frac{3}{2}\mu\Delta(N-1)(N-2) + \lambda(N-1) \right] + \Delta_N \left[\frac{3}{2}\mu\Delta(M-1)^2(M-2) + \lambda(M-1) \right] \\
&+ \frac{3}{2}\mu\Delta^2 \left(\frac{((M-1)(M-2))^2}{4} + \frac{(2N-3)(N-1)(N-2)}{6} \right) \\
&+ \lambda\Delta \left(\frac{(N-1)(N-2)}{2} + \frac{(M-1)(M-2)}{2} \right)
\end{aligned} \tag{17}$$

The difference between the proposed method and this alternative resides in the coefficients that multiply the terms in Δ_P and Δ_N . When $M \leq N$, looking at Equation 12, it emerges that our loss weighs more the positive error than the alternative constraint in Equation 17, thanks to the coefficients of Δ_P , which are smaller for the alternative loss.

D Additional training details

D.1 Network details

For the binary classification on the 3D MRI images, we employ a DNN architecture composed by two, identical and parallel structures. For each patient, one path of the NN processes the diffusion-weighted images and the other part processes the T2-weighted axial images. Each path consists of cascaded 3D convolution, 3D max-pooling, and activation functions. Finally, in the fully connected layer the outputs are concatenated, as the different modalities carry complementary information. In the binary classification on CIFAR10 and CIFAR100, we use ResNet-10 [17] trained for 100 epochs and Adam optimizer, without any learning rate schedule and a batch size of 64. The common hyperparameters are selected based on the best validation AUC of BCE. For the multi-class, long-tailed experiments we follow the setup used by [4], as it is a recent and acknowledged work from the state of the art, and we keep it consistent over the baselines and ALM experiments, for a fair comparison. Specifically, we use ResNet-32 [17] as our base network, and use stochastic gradient descent with momentum of 0.9, weight decay of 2×10^{-4} for training. The model is trained with a batch size of 128 for 200 epochs. We use an initial learning rate of 0.1, then decay by 0.01 at the 160th epoch and again at the 180th epoch.

D.2 Further details on hyperparameters

We search the hyperparameter space incrementally in order to slightly reduce the number of simulations we run for computational purposes. Common hyperparameters such as number of epochs, learning rate, batch size and patience for early stopping have been selected as explained in Section D. Then, these parameters are kept fixed for all the experiments. Next, for the baselines having specific hyperparameters, the search is carried out specifically for each dataset as well as for each class ratio, among those values proposed by the original papers (apart from W-BCE for which does not provide

specific guideline for setting the weight of the loss, thus we decided to set it proportionate to the class ratio N for minority class' samples). More specifically, for the baselines the following values are considered:

- margin m has been searched among $\{0.5, 2, 4\}$ for S-ML and A-ML
- exponent γ has been searched among $\{0.5, 1, 2\}$ for S-FL and A-FL
- weight coefficient m has been searched among $\{N/3, 2N/3, N\}$ for WBCE, being N the class ratio
- exponent β has been searched among $\{0.99, 0.999, 0.9999\}$ for cb-BCE

Once the hyperparameters of the baselines are set, we keep them fixed for ALM training. Then, we seek for the best hyperparameters for ALM. With the same logic, we perform a grid search with varying ρ and $\mu^{(0)}$. We choose $\mu^{(0)}$ from the set $\{10^{-7}, 10^{-6}, 10^{-5}, 10^{-4}, 10^{-3}\}$ and ρ from the set $\{2, 3\}$, but we found that selecting the smallest ρ always provided the best results. Once we find the best combination of μ and ρ based on the AUC on the validation set, we fix them and search for δ from the set $\{0.1, 0.25, 0.5, 1.0\}$ for the binary task and $\{0.05, 0.1\}$ for the multi-class set-up.

E Ensembling results for binary CIFAR10 and CIFAR100

In Tables 10 and 11 we report the test AUC obtained with ensembling (the same as Tables 1 and 2 of the main paper), along with the corresponding average and the standard deviation of AUC over the 10 runs, for both the binary CIFAR10 and CIFAR100 experiments. Comparing results in Tables 10 and 11 with those for the MRI dataset in Table 3 of the main paper, it is noticeable that the standard deviation is consistently larger for the MRI dataset, compared to CIFAR10 and CIFAR100, reflecting a higher uncertainty of the network on the predictions for this dataset [20].

Table 10: Avg AUC over 10 runs and the corresponding ensembled AUC (reported in the main paper) for CIFAR10 in binary classification.

Dataset	CIFAR10, imb. 100		CIFAR10, imb. 200	
Training method	Avg. AUC	Ens. AUC	Avg. AUC	Ens. AUC
BCE	82.0 ± 2.6	91.2	75.8 ± 4.0	87.3
S-ML	82.6 ± 2.4	91.7	75.6 ± 3.5	87.4
S-FL	82.7 ± 2.0	91.7	74.8 ± 3.4	85.7
A-ML	83.4 ± 2.3	92.4	76.2 ± 2.5	87.4
A-FL	82.9 ± 2.3	92.3	74.6 ± 4.1	86.2
CB-BCE	73.2 ± 2.0	78.3	70.2 ± 3.6	78.1
W-BCE	79.0 ± 2.9	87.4	68.7 ± 3.3	78.3
LDAM	78.1 ± 3.3	89.0	74.1 ± 3.4	86.4
MBAUC	70.2 ± 4.2	74.0	63.7 ± 3.9	67.9
ALM + BCE	83.6 ± 1.6	93.1	75.5 ± 3.3	86.7
ALM + S-ML	83.6 ± 1.7	92.5	76.4 ± 3.5	87.9
ALM + S-FL	82.2 ± 1.6	91.5	75.8 ± 3.3	86.9
ALM + A-ML	83.6 ± 2.1	92.8	76.5 ± 3.4	87.6
ALM + A-FL	82.7 ± 2.3	92.7	75.6 ± 3.7	87.0
ALM + CB-BCE	76.2 ± 5.3	88.1	71.6 ± 3.2	80.6
ALM + W-BCE	80.6 ± 1.9	89.3	72.2 ± 3.0	81.0
ALM + LDAM	80.0 ± 3.1	91.0	74.2 ± 2.7	85.6

Table 11: Avg AUC over 10 runs and the corresponding ensembled AUC (reported in the main paper) for CIFAR100 in binary classification.

Dataset	CIFAR100, imb. 100		CIFAR100, imb. 200	
Training method	Avg. AUC	Ens. AUC	Avg. AUC	Ens. AUC
BCE	77.8 ± 1.7	81.8	75.7 ± 3.6	79.1
S-ML	78.0 ± 2.5	82.7	75.4 ± 4.0	79.7
S-FL	78.2 ± 2.7	82.6	75.7 ± 3.6	80.1
A-ML	77.8 ± 1.7	81.8	75.8 ± 3.8	79.8
A-FL	78.1 ± 2.3	82.8	75.7 ± 3.4	80.1
CB-BCE	76.7 ± 1.6	78.8	74.9 ± 3.3	78.7
W-BCE	76.6 ± 1.6	79.7	76.4 ± 1.7	79.7
LDAM	77.6 ± 3.8	82.8	76.9 ± 2.4	82.1
MBAUC	79.7 ± 1.5	82.3	78.6 ± 1.6	80.3
ALM + BCE	78.6 ± 1.8	82.7	74.7 ± 4.3	80.9
ALM + S-ML	78.8 ± 1.8	81.7	74.9 ± 3.7	80.7
ALM + S-FL	78.0 ± 2.7	81.7	74.7 ± 3.8	80.8
ALM + A-ML	78.2 ± 2.4	82.7	76.4 ± 3.2	81.0
ALM + A-FL	77.9 ± 2.7	83.2	75.8 ± 2.9	80.8
ALM + CB-BCE	79.5 ± 1.6	83.8	77.7 ± 2.2	81.0
ALM + W-BCE	79.8 ± 0.8	83.2	76.5 ± 2.6	81.3
ALM + LDAM	77.8 ± 2.6	83.2	78.4 ± 2.1	81.5

F Statistical significance

All the results presented in the paper are obtained by averaging 10 runs with different random seeds for the model parameters. We perform statistical significance analysis on the AUC results using the DeLong test [9]. We copy the results of ALM below from Tables 1, 2, and 3 in the main paper and marked the ones that passes the DeLong test ($p \leq 0.5$) using *. Also, note that we wrote the results where ALM improves baseline using bold font. Therefore, a bold result marked with * indicates that the improvement achieved by ALM over the baseline is statistically significant which is the case in the majority of the cases shown in the Tables 12, 13 and 14.

Table 12: Statistical significance analysis on binary CIFAR10 for class ratio 1:100 and 1:200.

Dataset	Binary CIFAR10, imb. 100	Binary CIFAR10, imb. 200
Training method	AUC	AUC
ALM + BCE	93.1*	86.7
ALM + S-ML	92.5*	87.9*
ALM + S-FL	91.5	86.9*
ALM + A-ML	92.8	87.6*
ALM + A-FL	92.7*	87.0*
ALM + CB-BCE	88.1*	80.0*
ALM + W-BCE	89.3*	81.0*
ALM + LDAM	91.0*	85.6

Table 13: Statistical significance analysis on binary CIFAR100 for class ratio 1:100 and 1:200.

Dataset	Binary CIFAR100, imb. 100	Binary CIFAR100, imb. 200
Training method	AUC	AUC
ALM + BCE	82.7*	80.9*
ALM + S-ML	81.7	80.7*
ALM + S-FL	81.7	80.8*
ALM + A-ML	82.7*	81.0*
ALM + A-FL	83.2*	80.7
ALM + CB-BCE	83.8*	81.0*
ALM + W-BCE	83.2	81.3*
ALM + LDAM	83.2	81.5

Table 14: Statistical significance analysis on in-house MRI dataset.

Method	AUC ens.
ALM + BCE	85.4*
ALM + S-ML	80.3*
ALM + S-FL	84.2*
ALM + A-ML	76.4*
ALM + A-FL	81.5
ALM + CB-BCE	79.5
ALM + W-BCE	81.4*
ALM + LDAM	77.0*

G Results on MRI dataset at higher levels of False Negatives

In this Section we report the FPRs on the MRI dataset @2FN, and @5FN. Overall, it can be observed that the largest benefit from ALM is obtained at higher TPR, consistently with our goal.

Table 15: Results on in-house MRI dataset at higher FNRs.

Method	FPR @2 FN	FPR @5 FN
BCE	31.3	12.5
S-ML	37.5	9.4
S-FL	25.0	4.5
A-ML	26.6	4.5
A-FL	21.8	4.5
CB-BCE	23.4	1.6
W-BCE	32.8	4.5
LDAM	25.0	4.5
ALM + BCE	20.3	1.6
ALM + S-ML	21.8	1.6
ALM + S-FL	21.5	1.6
ALM + A-ML	21.8	4.5
ALM + A-FL	15.6	1.6
ALM + CB-BCE	21.5	1.6
ALM + W-BCE	21.8	1.6
ALM + LDAM	21.5	1.6

H Additional experiments at lower and consistent imbalances

In an earlier version of this work, we tested ALM on a smaller version of CIFAR10 and injected class imbalance with ratios 1:2, 1:9, and 1:19. Moreover, the previous setting presented a consistent imbalance among training, validation and test sets. We provide the results obtained from the previous study in the Table 16.

Table 16: Evaluation of results on CIFAR10 dataset. From top to bottom, results are shown for class ratio 1:2, 1:9, 1:19 with consistent imbalance across training, validation and test sets.

Training method	Test AUC	FPR @ 100% TPR	FPR @ 95% TPR	FPR @ 90% TPR
BCE	94.67	69.1	20.9	15.2
S-ML	94.57	68.2	21.6	15.2
S-FL	94.74	64.3	22.0	15.6
A-ML	94.56	67.0	21.8	15.6
A-FL	94.87	65.1	20.1	13.8
W-BCE	94.54	68.7	21.9	15.6
CB-BCE	94.38	69.3	23.5	16.3
MBAUC	94.26	69.6	23.80	15.40
ALM + BCE	95.41	66.2	21.1	<u>13.2</u>
ALM + S-ML	95.10	61.9	21.9	13.5
ALM + S-FL	95.22	54.3	20.5	14.7
ALM + A-ML	95.18	65.0	21.4	14.3
ALM + A-FL	94.95	64.0	20.5	14.7
ALM + W-BCE	<u>95.67</u>	59.9	18.7	<u>13.2</u>
ALM + CB-BCE	95.47	<u>58.8</u>	<u>18.5</u>	13.4
BCE	93.96	41.3	20.6	16.6
S-ML	94.04	39.6	20.3	16.2
S-FL	93.39	39.7	19.4	17.6
A-ML	93.64	42.1	21.3	17.3
A-FL	93.70	42.0	20.9	17.1
W-BCE	91.12	54.1	30.5	23.4
CB-BCE	90.83	58.5	31.7	27.1
MBAUC	92.04	44.1	22.7	17.0
ALM + BCE	94.74	34.2	19.9	14.1
ALM + S-ML	94.98	28.5	20.0	14.0
ALM + S-FL	94.2	35.6	22.5	17.4
ALM + A-ML	94.87	32.9	18.9	13.6
ALM + A-FL	<u>95.38</u>	<u>31.4</u>	<u>16.5</u>	<u>12.4</u>
ALM + W-BCE	93.03	47.9	23.1	19.8
ALM + CB-BCE	93.89	38.5	22.7	17.9
BCE	91.95	40.4	27.9	21.1
S-ML	92.28	36.4	27.9	22.0
S-FL	92.17	39.3	<u>23.5</u>	22.7
A-ML	91.74	34.2	27.4	22.6
A-FL	91.88	45.8	32.5	21.7
W-BCE	88.85	61.2	41.2	32.7
CB-BCE	88.24	61.6	36.5	35.1
MBAUC	91.8	36.00	26.4	25.0
ALM + BCE	93.21	29.8	27.5	17.2
ALM + S-ML	93.76	<u>28.4</u>	24.1	17.9
ALM + S-FL	93.50	31.0	23.5	16.8
ALM + A-ML	93.06	29.0	26.2	22.4
ALM + A-FL	93.45	34.4	27.7	22.3
ALM + W-BCE	91.22	48.2	31.2	19.6
ALM + CB-BCE	90.80	52.6	42.1	25.7